# Design of a Dual-Band Doherty Power Amplifier Utilizing Simplified Phase Offset-Lines

**Xuan Zheng[1, 2], Yuanan Liu[1, 2], Cuiping Yu[1, 2], Shulan Li[1, 2], and Jiuchao Li[1, 2, *]**

**Abstract**—This paper proposes a novel design methodology for dual-band Doherty power amplifier (DPA) with simplified offset-lines. The methodology is validated with the design and fabrication of a 10 W GaN based DPA for Global System for Mobile Communications (GSM) and Wideband Code Division Multiple Access (WCDMA) applications at 0.90 GHz and 2.14 GHz, respectively. In the measurement results, the DPA achieves a drain efficiency (DE) of 51.2% with an output power of 37.2 dBm at the 6.5 dB output power back-off (OBO) from the saturated output power at 0.90 GHz, and a DE of 39.9% with an output power of 37.4 dBm at the 6.5 dB OBO at 2.14 GHz. Linearity results using 20 MHz 16 QAM signal show an adjacent channel leakage ratio (ACLR) of −48 dBc and −43 dBc with the average output power of 37.2 dBm and 37 dBm at 0.90 GHz and 2.14 GHz, respectively.

## 1. INTRODUCTION

With the development of modern communication technologies, mobile communication systems have to accommodate multiple standards simultaneously, for instance, GSM, CDMA, WCDMA, WiMax, which operate at different frequency bands. This requirement has increased the demand for multi-band RF components, including RF power amplifiers (PAs). One straightforward solution is to utilize several single band PAs in parallel, which not only costs a lot, but also results in significant power loss. Therefore, it is quite essential to study and develop multi-band PAs. In 2002, Chow and Wan proposed a two-section 1/3-wavelength transformer line operating at the fundamental frequency and its first harmonic frequency [1], which propels the evolution of dual-band impedance transforming. Then the structure was enhanced in order to operate at two independent frequencies [2]. From then on, many efforts have been made to develop dual-band PAs [3–5].

The performance of PA does matter a lot due to its huge power-consumption among the communication systems. In other words, the efficiency and linearity of the PAs largely determine the performance of the whole base station. However, Class AB, Class B, and Class C PAs reach their highest efficiency at the saturation point, while the efficiency is low at lower output power. It is not satisfactory especially when the signals with high peak-to-average power ratio (PAPR) are widely utilized because of the popular usage of non-constant envelope modulation schemes in order to pursue high transmission capacity. To solve the problem, DPA was first proposed by Doherty in 1936 [6] and developed towards several meaningful directions later [7–9], and one of them is the dual-band DPA [10–16], which perfectly meets the requirements of modern communications. In 2010, a dual-band DPA was proposed and focused on the passive structures involved in the DPA design, whose drain efficiencies achieve 45% when the output power is between 33 dBm and 39 dBm at both 2.14 GHz and 3.5 GHz [12]. In 2011, a novel accurate dual-band phase offset-line was proposed and proved to be quite useful for the design of the dual-band DPA, whose peak drain efficiencies reach 42.1% and 36.8% with the output

\* Corresponding author: Jiuchao Li (lijiuchao@gmail.com).
[1] Beijing Key Laboratory of Work Safety Intelligent Monitoring, Beijing University of Posts and Telecommunications, Beijing, China.
[2] School of Electronic Engineering, Beijing University of Posts and Telecommunications, Beijing, China.

power of 38 dBm at 1.96 GHz and 3.5 GHz, respectively [13], while the structure is too complicated to implement relatively.

In this paper, a 0.90/2.14 GHz dual-band DPA is designed and implemented with much simpler offset-lines than usual, which are used to optimize the performance of this piece and finally validated with simulation, hardware design and measurements. The measured peak DEs are 67.0% and 57.3% together with peak output powers of 43.7 dBm and 43.9 dBm, respectively. And the drain efficiencies exceed 51.2% and 39.9% over 6.5 dB OBO region from the saturation.

## 2. DUAL-BAND DOHERTY POWER AMPLIFIER TOPOLOGY

Just like the conventional DPA, the dual-band DPA is composed of a carrier amplifier and a peaking amplifier, which are biased at Class AB and Class C, respectively. Figure 1 shows the block diagram of the proposed dual-band DPA, including an input power divider, input/output impedance matching networks, phase offset-lines and two different impedance inverters. In order to implement a dual-band DPA, all the components in the topology should be judiciously designed to satisfy the dual-band characteristic and requirements. The design approach of each element is discussed detailedly as follows.
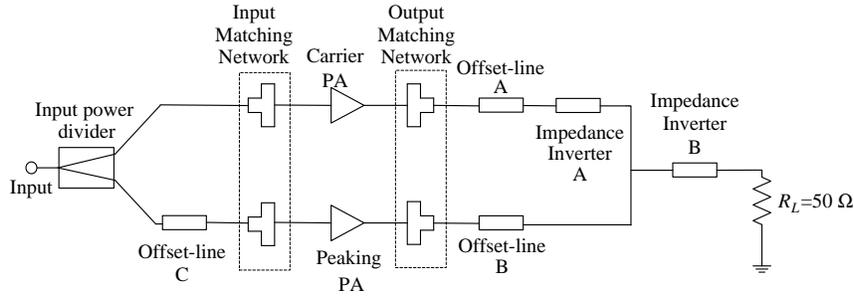


**Figure 1.** The block diagram of the proposed Doherty power amplifier.

### 2.1. Input Power Divider

In order to design a DPA, the input power needs to be divided and sent to the carrier and peaking amplifier. Uneven power division benefits the DE or the linearity of the PA depending on the power-ratio, while the equal division is much less complicated to carry out. In this paper, an even Wilkinson divider is adopted compromising both the performance of the DPA and the manufacturing complexity, the detailed design equations of the divider have been rigorously derived in [17].

### 2.2. Impedance Matching Network

The dual-band output matching network ensures that the PA exports the maximum power, and the input matching section ensures an appropriate gain. For the sake of the design complexity, the carrier and peaking amplifiers adopt a greatly identical matching network, i.e., a three-section microstrip transformer for frequency-dependent complex load impedance, which matches complex impedance to real one at both operating frequencies simultaneously. The specific closed-form solutions for this transformer can be found in [18].

### 2.3. Impedance Inverter

The traditional quarter-wave impedance inverter is a narrow band supporter, not satisfying the impedance inverting at both operating frequencies. Therefore, some extended dual-band inverters are proposed, such as T- or $\pi$-network.

In [19], it is shown that an equivalent quarter-wavelength transmission line of characteristic impedance $Z_0$, at two incommensurate frequencies $f_1$ and $f_2$, can be realized by using a T- or $\pi$-network. By equalling the two $ABCD$ matrices of this framework and the conventional quarter-wave
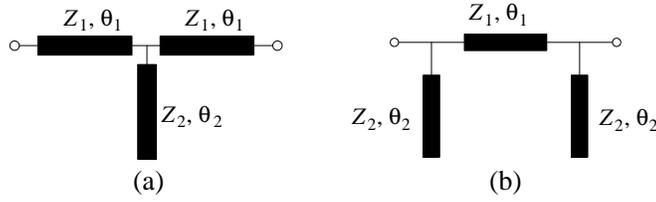
**Figure 2.** Dual-band quarter-wave impedance inverter, (a) T-network and (b) $\pi$-network.

transmission line at both required frequencies, the design parameters are easy to obtain. Figure 2 elucidates the scheme, which is composed of two identical microstrips and another different one. The design equations for the two structures are given in [19, 20] as functions of the operating frequencies $f_1$ and $f_2$ and of the equivalent characteristic impedance $Z_0$.

## 3. DESIGN AND IMPLEMENTATION OF THE DUAL-BAND DPA

In this section, the design of a dual-band DPA for 0.90 GHz and 2.14 GHz is presented. As to both carrier and peaking amplifiers, a hybrid GaN HEMT device, Cree CGH40010 has been used, whose nonlinear model is supplied by the manufacturer and optimized for Class AB biasing condition. The stability circuit is designed according to the datasheet of the device and optimized by simulation.

The load-pull/source-pull simulation has been performed for each of the frequencies, and the result is shown in Table 1. Then the output/input matching design is finally configured by solving the parameters of the three-section transformer.

The offset-line A is set to double the optimum output impedance of the carrier amplifier when the DPA operating at low input power especially at the 6 dB OBO, while it causes no influence on the performance at saturated power. To be specific, the offset-line is supposed to have the characteristic impedance of 50 $\Omega$, and also ought to achieve the transformation at the low input power from 100 $\Omega$ to a certain impedance $Z'_{\mathrm{opt}}$, and the value of which will decide the power-added efficiency (PAE) at the 6 dB OBO. Therefore, the designer should choose an appropriate $Z'_{\mathrm{opt}}$ depending upon the PAE contours simulated by the software. Once the impedance is determined, the electronic length of the offset-line is also decided. As the two required optimum lengths for the two frequencies are usually irrelevant, various complicated networks are designed to realize the arbitrary phase shift at dual-band operation. However, there is another way to pursue the famous electronic length. Assuming that the ratio of the two operating frequencies is $f_1/f_2$ and since the lengths are chosen by the designer, it is possible to make the ratio of the two required electronic lengths approximately equal to $f_1/f_2$ at the cost of PAE. In this way, the only rule the designer needs to concern about is to turn down the loss of PAE as much as possible. In this paper, the length of the offset-line A is finally verified by simulation, which performs 175° at 0.90 GHz and 56° (416°–360° = 56°) at 2.14 GHz (175/416 $\approx$ 0.90/2.14). Figure 3 makes the operating procedure of the offset-line A clear, (a) shows the transforming path at 0.90 GHz,

**Table 1.** Design parameters of the proposed dual-band DPA.

| Amplifier | Parameter | Symbol | Value |
|---|---|---|---|
| Carrier Amplifier | DC Bias Current | $I_{\mathrm{DC,Carrier}}$ | 200 mA |
| | DC Gate Voltage | $V_{\mathrm{GG,Carrier}}$ | $-2.75$ V |
| | Load Impedance @ $f_1$ | $Z_{\mathrm{Opt1,Load}}$ | $28.9 + j10.6\,\Omega$ |
| | Load Impedance @ $f_2$ | $Z_{\mathrm{opt2,Load}}$ | $18.1 + j4.9\,\Omega$ |
| | Source Impedance @ $f_1$ | $Z_{\mathrm{opt1,Source}}$ | $47.7 - j55.1\,\Omega$ |
| | Source Impedance @ $f_2$ | $Z_{\mathrm{opt2,Source}}$ | $11.5 - j11.0\,\Omega$ |
| Peaking Amplifier | DC Gate Voltage | $V_{\mathrm{GG,Peaking}}$ | $-4.85$ V |

and the impedance is transformed from $100\,\Omega$ to $97.8 + j12.7\,\Omega$, the PAE of which is 3% lower than the peak, (b) shows the transforming path at $2.14\,\text{GHz}$, and the impedance is transformed from $100\,\Omega$ to $32.7 - j22.7\,\Omega$, the PAE of which is 2% lower than the peak. It can be easily understood that the sacrifice of the PAEs is both negligible and quite acceptable.

Offset-line B is set to imitate the open circuit situation in case of power leakage from the carrier amplifier when the peaking one shuts off at low input power. And its length is optimized to transform the impedance here to a certain value as huge as possible at both frequencies. Obviously, the simplified offset-line, i.e., a single-band transmission line, is applicable to dual-band PA design. Through this strategy, the design complexity of dual-band PA is significantly reduced, though the PAEs at back-off level are inevitably compromised to some extent. The offset-line C, a T-shape dual-band inverter, is synthesized to compensate the phase difference between the two outputs.

The dual-band Wilkinson power divider and dual-band impedance inverters are configured in accordance with the methodology mentioned in Section 2. Impedance inverter A acts like a dual-band quarter-wave inverter owning characteristic of $50\,\Omega$, while B performs as another dual-band quarter-wave inverter owning characteristic of $35\,\Omega$ and accomplishes the inverting from $25\,\Omega$ to $50\,\Omega$ all the time. The final entire DPA is implemented on the substrate of Rogers 4350B with relative dielectric constant of 3.48 and substrate thickness of 30 mil whose prototype is displayed in Figure 4.
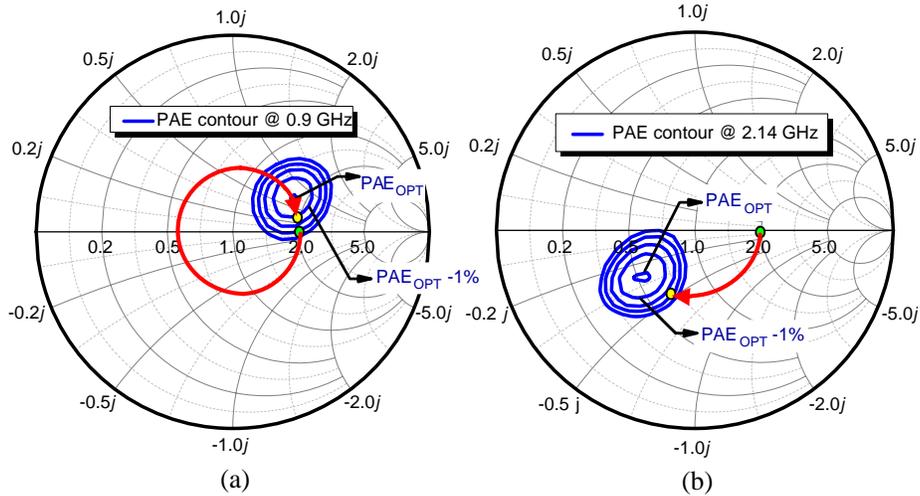


**Figure 3.** Carrier phase offset-line (offset-line A) operating path, (a) $0.90\,\text{GHz}$ and (b) $2.14\,\text{GHz}$.
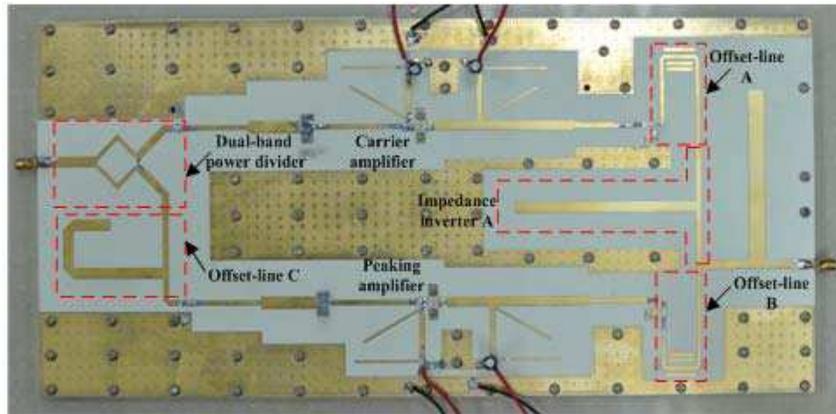


**Figure 4.** Prototype of the proposed dual-band DPA.

## 4. MEASUREMENT RESULTS

The dual-band DPA has been characterized by small-signal, large-signal and modulated-signal measurements to evaluate its performance.

### 4.1. Small-signal Measurement

The small-signal condition is well used to characterize the frequency behavior of the PA. In this work, the supply voltages of the carrier and peaking PAs are both set to 28 V with the gate bias voltages setting as $-2.75$ V and $-4.85$ V, respectively. Thus the carrier amplifier possesses a quiescent drain current of 200 mA. The simulated and measured scattering parameters of the carrier amplifier are reported in Figure 5, revealing a strong agreement and a perfect matching situation. As the peaking amplifier adopts the same circuit structure as the carrier one, its small-signal performance is also verified by Figure 5.

### 4.2. Large-Signal Measurement

Large-signal continuous wave (CW) measurement has been performed to evaluate the performance of the DPA under steady-state conditions. In this measurement, the same biasing, as for the $S$-parameters measurement, is utilized for the dual-band DPA, whose results are plotted in Figure 6. The peak output power is 43.7 dBm and 43.9 dBm with the drain efficiencies of 67.0% and 57.3% for 0.90 GHz and 2.14 GHz, respectively. The drain efficiencies are higher than 51.2% and 39.9% over the 6.5 dB
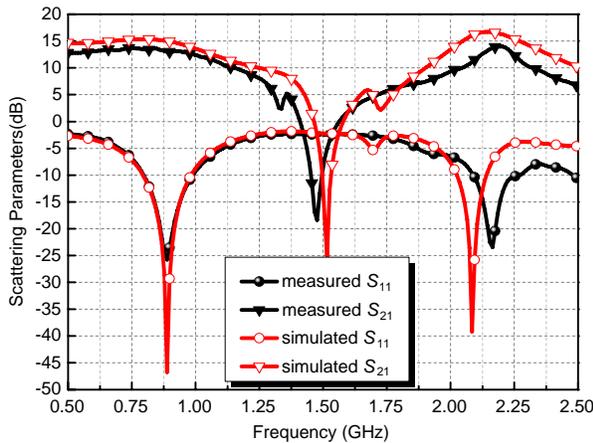


**Figure 5.** Measured and simulated $S$-parameters of the carrier amplifier.
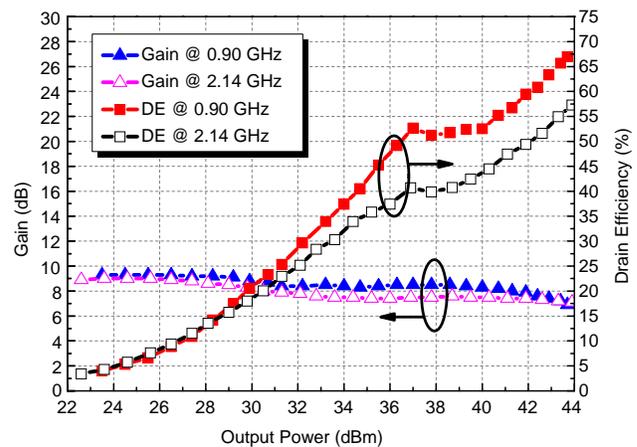
**Figure 6.** Measured gain and DE of the DPA versus output power at the operating bands.

**Table 2.** Performance comparison of 2-way dual-band Doherty PAs.

| PA | year | Device (C/P) | Frequency (GHz) | Saturated power at $f_1/f_2$ (dBm) | DE at $f_1/f_2$ (%) |
|---|---|---|---|---|---|
| [10] | 2010 | SiC (60/60 W) | 0.90/2.0 | 41.9/41.2 | 39.8/41.4 @ 5 dB OBO |
| [11] | 2011 | SiC (10/10 W) | 0.88/1.96 | 35/35 | 33/30 @ 6 dB OBO |
| [12] | 2011 | GaN (5/5 W) | 2.14/3.5 | 39/39 | 44/45 @ 6 dB OBO |
| [13] | 2011 | GaN (10/10 W) | 1.96/3.5 | 42.7/41.8 | 42.1/36.8 @ 6.5 dB OBO |
| [14] | 2012 | GaN (15/15 W) | 1.8/2.4 | 43/43 | 60/44 @ 6 dB OBO |
| [15] | 2012 | GaN (10/10 W) | 2.14/2.655 | 43/43 | 45/40 @ 4 dB OBO |
| [16] | 2013 | GaN (10/10 W) | 0.85/2.33 | 44/42.5 | 45/41 @ 6 dB OBO |
| This work | 2013 | GaN (10/10 W) | 0.90/2.14 | 43.7/43.9 | 51.2/39.9 @ 6.5 dB OBO |

OBO region for 0.90 GHz and 2.14 GHz. The gains for the operating frequencies are 9.3 dB and 8.9 dB, which are set a little lower than common designs in order to pursue much higher peak output power.

Table 2 describes the comparison of some published dual-band DPAs. From the table, it can be seen that this work achieves the highest peak output power at both frequencies and shows performance improvements in terms of efficiency as well as operating frequency spacing compared with some of the previous structures.

### 4.3. Modulated-Signal Measurement

Linearized modulated measurement has been carried out to prove the capability of the DPA being linearized and to evaluate its performance when used with modern wireless communication signals. The test results are displayed in Figure 7, when the DPA was driven with the 20 MHz 16 QAM signal at the average output power of 37.2 dBm and 37.0 dBm with and without digital pre-distortion (DPD) at both 0.90 GHz and 2.14 GHz. Besides that, it is also tested by 10 MHz and 40 MHz 16 QAM signals, whose details including average output power, ACLR with and without DPD are all shown in Table 3, which shows that all the measured ACLR with DPD are better than $-40$ dBc, which is superior for the communication systems. In other words, from the measurement results, it can be easily understood that this proposed work is experimentally validated to achieve a good linearity performance at both operating frequencies.
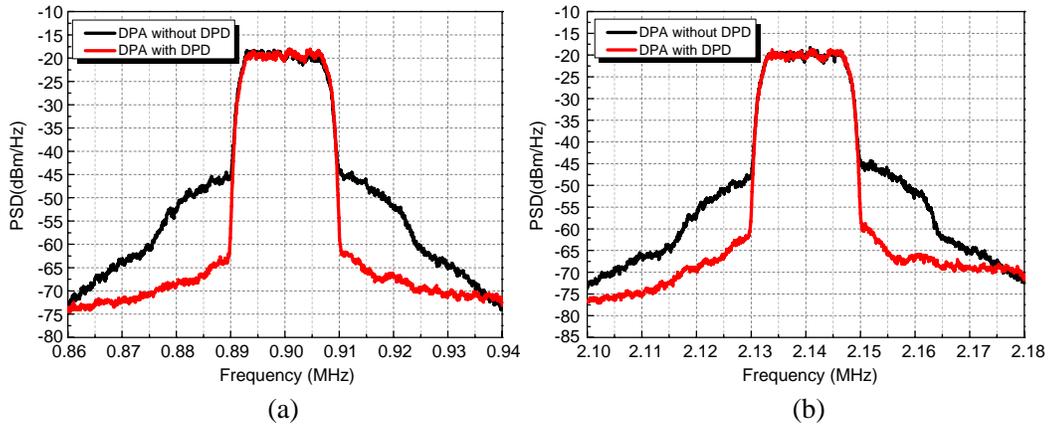


**Figure 7.** DPA output signal spectrum of a 20- MHz 16 QAM signal, (a) 0.90 GHz, (b) 2.14 GHz.

**Table 3.** Linearization results with different methods.

| Frequency (GHz) | Signal | Average output power (dBm) | ACLR (dBc) | |
| --- | --- | --- | --- | --- |
| | | | $w/o$ DPD | $w$ DPD |
| 0.90 | 10 MHz 16 QAM | 37.3 | $-31.2/-31.5$ | $-46.1/-46.5$ |
| 0.90 | 40 MHz 16 QAM | 36.7 | $-30.2/-31.1$ | $-43.2/-43.2$ |
| 2.14 | 10 MHz 16 QAM | 36.8 | $-31.8/-30.2$ | $-43.2/-43.1$ |
| 2.14 | 40 MHz 16 QAM | 36.5 | $-30.5/-28.6$ | $-43.6/-40.2$ |

### 5. CONCLUSION

In this work, a dual-band DPA with optimized phase offset-lines whose simplified structure contributes to the reduction of the whole design complexity is proposed and deduced. The proposed design methodology to synthesize some passive dual-band components is proved to be applicable and effective in the implementation of the dual-band 0.90/2.14 GHz Doherty power amplifier. The measured peak

output power exceeds 43.7 dBm at both operating frequencies. And the drain efficiencies are higher than 51.2% and 39.9% over the 6.5 dB output power back-off region from the power saturation point at 0.90 GHz and 2.14 GHz, respectively. Moreover, 16 QAM signals with different bandwidths are applied to test the linearization performance, one of which is 20 MHz 16 QAM signal test, and the measured ACLR at the average output power in this situation is better than −48 dBc and −43 dBc at 0.90 GHz and 2.14 GHz. Overall, the proposed dual-band Doherty PA combining advantages including dual-band, high efficiency, and low-complexity meets the requirements of communication systems perfectly, and can be introduced to most of dual-band transceiver systems, primarily in base-stations considering the power level and dimension, but the design methodology is also available in mobile phones after some efforts on miniaturization, like on-chip design. As can be seen from the above, the proposed dual-band Doherty PA has great potential for the modern wireless communication systems, and a bright future of the design is definitely clear.

## ACKNOWLEDGMENT

## REFERENCES

1. Chow, Y. L. and K. L. Wan, "A transformer of one-third wavelength in two sections — For a frequency and its first harmonic," *IEEE Microwave and Wireless Components Letters*, Vol. 12, No. 1, 22–23, 2002.
2. Monzon, C., "A small dual-frequency transformer in two sections," *IEEE Transactions on Microwave Theory and Techniques*, Vol. 51, No. 4, 1157–1161, 2003.
3. Colantonio, P., F. Giannini, and L. Scucchia, "A new approach to design matching networks with distributed elements," *15th International Conference on Microwaves, Radar and Wireless Communications, MIKON-2004*, Vol. 3, 811–814, 2004.
4. Ji, S. H., C. S. Cho, J. W. Lee, and J. Kim, "Concurrent dualband class-E power amplifer using composite right/left-handed transmission lines," *IEEE Transactions on Microwave Theory and Techniques*, Vol. 55, No. 6, 1341–1347, 2007.
5. Chuang, M. L., "Dual-band impedance transformer using two-section shunt stubs," *IEEE Transactions on Microwave Theory and Techniques*, Vol. 58, No. 5, 1257–1263, 2010.
6. Doherty, W. H., "A new high efficiency power amplifier for modulated waves," *Proceedings of the Institute of Radio Engineers*, Vol. 24, No. 9, 1163–1182, 1936.
7. Yang, Y., J. Cha, B. Shin, and B. Kim, "A fully matched $N$-way Doherty amplifier with optimized linearity," *IEEE Transactions on Microwave Theory and Techniques*, Vol. 51, No. 3, 986–993, 2003.
8. Srirattana, N., A. Raghavan, D. Heo, P. E. Allen, and J. Laskar, "Analysis and design of a high-efficiency multistage Doherty power amplifier for wireless communications," *IEEE Transactions on Microwave Theory and Techniques*, Vol. 53, No. 3, 852–860, 2005.
9. Wood, J., M. LeFevre, D. Runton, J. C. Nanan, B. H. Noori, and P. H. Aaen, "Envelope-domain time series (ET) behavioral model of a Doherty RF power amplifier for system design," *IEEE Transactions on Microwave Theory and Techniques*, Vol. 54, No. 8, 3163–3172, 2006.
10. Li, X., W. Chen, Z. Zhang, Z. Feng, X. Tang, and K. Mouthaan, "A concurrent dual-band Doherty power amplifier," *IEEE Microwave Conference Proceedings (APMC)*, 654–657, 2010.
11. Colantonio, P., F. Feudo, F. Giannini, R. Giofre, and L. Piazzon, "Design of a dual-band GaN Doherty amplifier," *2010 18th International Conference on Microwave Radar and Wireless Communications (MIKON)*, 1–4, 2010.
12. Bassam, S. A., W. Chen, M. Helaoui, F. M. Ghannouchi, and Z. Feng, "Linearization of concurrent dual-band power amplifier based on 2D-DPD technique," *IEEE Microwave and Wireless Components Letters*, Vol. 21, No. 12, 685–687, 2011.

13. Rawat, K. and F. M. Ghannouchi, "Design methodology for dual-band Doherty power amplifier with performance enhancement using dual-band offset lines," *IEEE Transactions on Industrial Electronics*, Vol. 59, No. 12, 4831–4842, 2012.

14. Saad, P., P. Colantonio, L. Piazzon, F. Giannini, K. Andersson, and C. Fager, "Design of a concurrent dual-band 1.8–2.4-GHz GaN-HEMT Doherty power amplifier," *IEEE Transactions on Microwave Theory and Techniques*, Vol. 60, No. 6, 1840–1849, 2012.

15. Grebennikov, A. and J. Wong, "A dual-band parallel Doherty power amplifier for wireless applications," *IEEE Transactions on Microwave Theory and Techniques*, Vol. 60, No. 10, 3214–3222, 2012.

16. Chen, W., S. Zhang, Y. Liu, and F. M. Ghannouchi, "A concurrent dual-band uneven Doherty power amplifier with frequency-dependent input power division," *IEEE Transactions on Circuits and Systems I: Regular Papers*, Vol. 61, No. 2, 552–561, 2014.

17. Park, M. J. and B. Lee, "Wilkinson power divider with extended ports for dual-band operation," *Electronics Letters*, Vol. 44, No. 15, 916–917, 2008.

18. Liu, X., Y. A. Liu, S. L. Li, F. Wu, and Y. L. Wu, "A threesection dual band transformer for frequency-dependent complex load impedance," *IEEE Microwave and Wireless Components Letters*, Vol. 19, No. 10, 611–613, 2009.

19. Zhang, H. and K. J. Chen, "A stub tapped branch-line coupler for dual-band operations," *IEEE Microwave and Wireless Components Letters*, Vol. 17, No. 2, 106–108, 2007.

20. Cheng, K. K. and F. L. Wong, "A novel approach to the design and implementation of dual-band compact planar 90° branch-line coupler," *IEEE Transactions on Microwave Theory and Techniques*, Vol. 52, No. 11, 2458–2463, 2004.